Thin–Walled Structures 215 (2025) 113445

Contents lists available at ScienceDirect

Thin-Walled Structures

journal homepage: www.elsevier.com/locate/tws

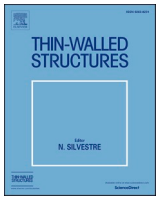

Full length article

Local buckling load of a perforated plate – A computational study

Elenor Naraidoo [a,*], Barbara Rossi [a,b]

[a] University of Oxford, Department of Engineering Science, UK
[b] KU Leuven, Department of Chemical Engineering, Belgium

ARTICLE INFO

Keywords:
Buckling
Perforations
Predicting equations

ABSTRACT

The webs of thin-walled beams and columns can be perforated for aesthetic, maintenance or structural purposes, affecting the elastic buckling behaviour when subject to compression. When conservatively approximated as a simply-supported plate, the web may exhibit one of four local buckling modes. These modes may interact, akin to the interaction of global, distortional and local buckling observed in thin-walled columns. Accounting for this, five subsets of buckling deformation are defined and used to develop an algorithm, which determines the corresponding buckling mode depending on geometrical limits. These modes are Whole Plate Buckling (WPB), Unstiffened Strip Buckling (USB), Euler Strip Buckling (ESB), Lateral Perforation Buckling (LPB), or an interaction of these (INT). For each mode, a predicting equation for the critical elastic buckling load is proposed and compared to the critical elastic buckling load determined with the Finite Element Method (FEM). The mean ratio of the elastic buckling load for a perforated plate found with FEM to that predicted with the proposed formulae is 1.00 for 775 models, with an overall R^2 coefficient of 0.840. Finally, a reliability assessment determines a statistical model factor γ for a 95 % confidence interval. This factor is found for each local buckling mode, and proposed as 1.17 for all plates with any number of perforations, not exhibiting LPB.

1. Introduction to perforated plate buckling modes

In structural engineering, buckling is the sudden deformation (bifurcation) of a component (e.g. plate buckling) under compressive load. The deflection modeshape is characterised by buckling waves; the wavelength is dependent on the type of buckling, which in turn depends on the component's geometry and boundary conditions. For a column with a given cross-section, Euler buckling depends solely on the column buckling length. Conversely, plates are susceptible to local buckling which depends on the length to width (aspect) ratio. Often thin-walled section columns fail through an interaction of several buckling modes [1–3] such as local buckling, distortional buckling, global (flexural or torsional) buckling or any combination of those. Additionally, perforations cause changes to the stress distribution within a thin plate. Subsequently, local buckling of a plate with a series of perforations can arise in one of four modes, and a fifth interaction mode. These modes are defined as Whole Plate Buckling (WPB), Lateral Perforation Buckling (LPB), Unstiffened Strip Buckling (USB), and Euler Strip Buckling (ESB); they are dependent on the number, size, and location of perforations (Fig. 1). The nomenclature for these buckling modes is available in various publications [3–5] although diagrams and dimensional criteria specifying the causes of each mode are often vague or absent.

The relationship between the perforation dimensions and the elastic buckling load of a perforated plate depends on how buckling manifests; this influences whether the elastic buckling load may be greater or less than the elastic buckling load of an unperforated plate. As the elastic buckling load and modeshape are inter-related, this paper establishes an algorithm to determine the perforated plate local buckling mode, and a predicting equation for the elastic buckling load is proposed for each corresponding mode.

2. Literature review

2.1. Standardised prediction methods

The Direct Strength Method (DSM) is an established approach within the North American Specification for the Design of Cold-Formed Steel Structural Members [6], Australian and New Zealand standard for Cold-formed steel structures [7], and The Design of Cold-Formed Stainless Steel Structural Members in South African standard [8].

However, DSM is not immediately applicable to plated members with perforations, and semi-analytical approaches are necessary to

* Corresponding author.
E-mail address: elenor.naraidoo@pmb.ox.ac.uk (E. Naraidoo).

https://doi.org/10.1016/j.tws.2025.113445
Received 24 January 2025; Received in revised form 8 May 2025; Accepted 12 May 2025
Available online 21 May 2025

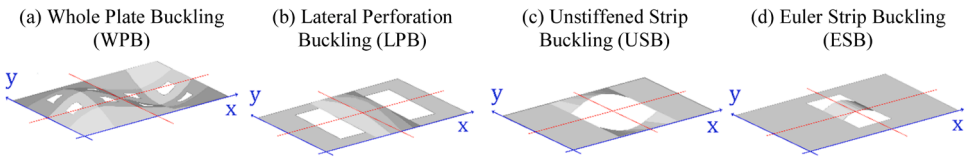

Fig. 1. Local buckling modes of perforated plates.

account for these. This may involve considering a weighted average thickness at the hole location with the Finite Strip Method (FSM), modelling the net section, or by recalculating the buckling strengths with Finite Element (FE) analysis. However, there are issues with each of these approaches which respectively may not accurately represent the cross-section rigidity, can lead to artificially high predictions for the local elastic buckling load, or are time consuming [9].

Chinese National Standard [10] and Eurocode 3 [11] propose the use of the effective width method for certain perforations. Eurocode 3 [11] requires that the size of the unstiffened hole does not exceed 5 % of the plate width, and such cases should be analysed with FE methods. Furthermore, Eurocode 3 [11] includes no consideration for the elastic buckling load of plates with multiple perforations. Chinese National Standard [10] provides specific criteria for different perforation sizes, spacings and arrangements permissible to limit their effect on the member's buckling resistance; the effective width of the flange or web is reduced relative to these geometries. However, the effective width method is only accurate where there is relatively little disruption to the load path within a plate, and it cannot be used for an irregular arrangement of perforations.

2.2. Research prediction methods

The derivation and solution of equilibrium equations to assess the buckling load of plates with multiple perforations is complex, time consuming and computationally demanding. Many authors parametrically assess the buckling load of perforated sections with commercial FE software. Some authors use these results to present design charts within a given domain [12], or discuss observations qualitatively [13,14], however most derive empirical relations, or suggest modifications to existing methods.

The effect of the total perforation width and area on the ultimate strength of thermal studs is investigated by [15] who recommend an equivalent thickness for the effective width method. Yao, Li and Guo [16] investigate the effect of increasing the spacing to diameter ratio of a concentric linear arrangement of circular holes on the elastic buckling of thin plates to recommend alternative elastic buckling coefficients. Brando and De Matteis [17] and Bernuzzi and Maxenti [18] respectively investigate angles with circular perforations and perforated pallet rack sections to recommend revisions to European design standards. Yao and Rasmussen [19] conduct an extensive parametric study on C-sections with a concentric linear arrangement of rectangular perforations of varied dimensions. The authors conduct a regression analysis on these results [19] and provide modification factors to the DSM equations proposed by [20] for American design standards [6].

Adany [21] investigates the application of the constrained finite element method (cFEM) for the buckling analysis of thin-walled members with holes. The author numerically investigates the influence of holes of various shapes and sizes on the global, distortional and local buckling modes. Modal decomposition with cFEM can determine hole-induced changes, where otherwise the effect of holes on the buckling behaviour can make it "all but impossible to reasonably assess the change of the critical load due to holes" [21].

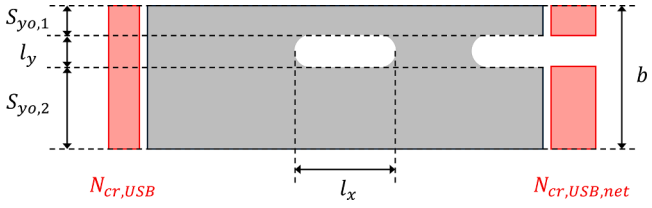

Fig. 2. Variables considered by [3].

Other authors establish analytical or semi-analytical methods. Semi-analytical methods informed in conjunction with FE procedure, are proposed by [4,22] and [23]. It is worth noting that [6] refers to research completed by [4] to determine the elastic buckling load of members with 'patterned holes' which are defined as small and tightly spaced, in a regular array of rows and columns for the complete length of a member. The authors propose that the critical elastic buckling load including the influence of perforations (N_{cr}) be determined as:

$$N_{cr} = \min\left(N_{cr,l,tr}, N_{cr,l,h}\right) \tag{1}$$

The load $N_{cr,l,h}$ is calculated using FSM of the net cross-section, with deformations restrained to local buckling, and examining only the buckling half-wavelengths shorter than the hole [24]. This is representative of lowest load that causes buckling within the length of a single perforation (USB or ESB) [4]. The load $P_{cr,l,}$ is determined with FSM for the complete length of the member, by reducing the thickness of each stiffened element in a cross-section containing perforation patterns to:

$$t_r = t\left[1 - \frac{n_r n_c (lh + \upsilon h\alpha + \upsilon l\beta + \alpha\beta)}{ab}\right]^{1/2} \tag{2}$$

where n_r is the number of perforations over the plate length, n_c is the number of perforations over the plate width, l is the length of the perforation, h is the height of the perforation, υ is the Poisson's ratio and α and β are perforation dimension modification factors accounting for the size of the perforation relative to the size of the buckled deformations [4].

Minera et al. [22] establish the Localised Nominal Stiffness method (LNS) to determine the sensitivity of a localised region of a structure to stiffness variation, i.e. the introduction of a hole. The result is a sensitivity contour map which informs the user where best to locate a small number of small holes. Gracia and Rammerstorfer [23] similarly develop a sensitivity contour map according to the vulnerability of a localised region to strain energy variation. Their map shows areas where the introduction of a small perforation can increase the elastic buckling load of a square plate.

Analytical predictions are achieved by considering a simplified mathematical problem [3,25,26]. Naraidoo, You and Rossi [25] derived a prediction for the buckling of a plate of any aspect ratio with any arrangement of perforations by solving Rayleigh's quotient for the minimum energy state of equilibrium. The authors assume that the additional strain energy is a uniform function of the applied force, and that the modeshape exhibits little change to that of the unperforated plate. It is found to be particularly accurate when the average centroid of all perforations is approximately equal to the location of the buckling antinode, and inaccurate for tall perforations, or perforations with a large aspect ratio. Scheperboer, Efthymiou and Maljaars [26] examine the buckling of square plates with staggered circular perforations and propose that elastic buckling load is a quadratic function of hole area and unperforated plate buckling load. They find that, for the same total perforation area, plates with more holes have lower buckling load. Thus,

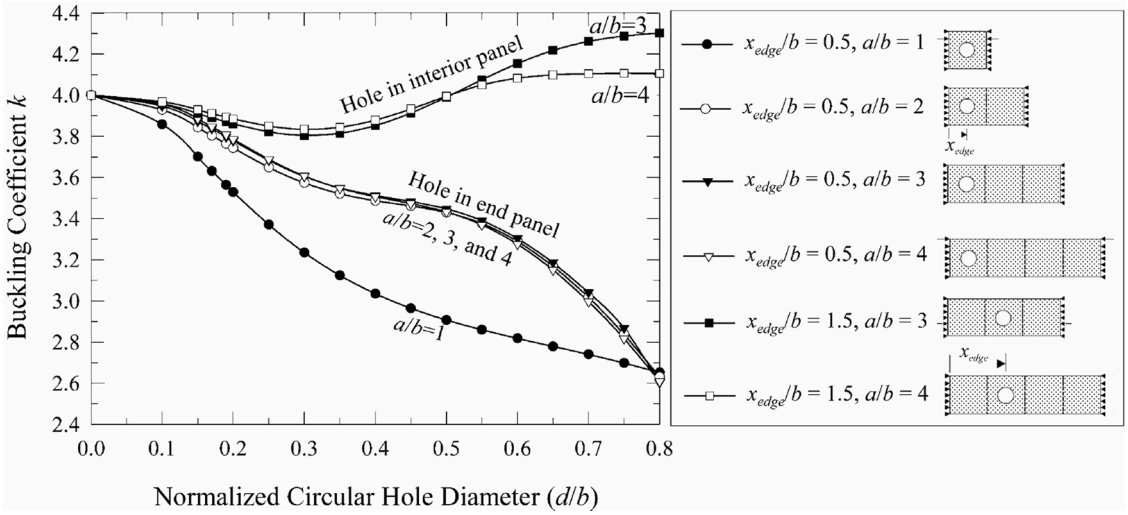

Fig. 3. Buckling coefficient (k) when the centre of a circular hole lies along the plate major axis and at a buckling maximum, reproduced from [32].

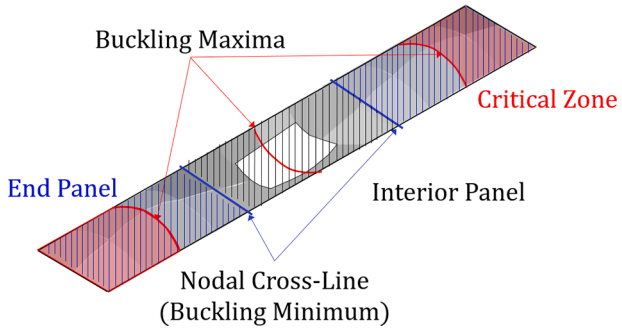

Fig. 4. Areas of a buckling plate.

they focus on parametric models with the most perforations to derive the equation's coefficients using the least square error method:

$$\frac{N_{cr}}{N_0} = 1.8(r_p)^2 - 2.1r_p + 1 \tag{3}$$

where the critical elastic buckling load of a perforated plate (N_{cr}) is a function of the critical elastic buckling load of an equivalent unperforated plate (N_0), and the ratio of the area of holes to the area of the unperforated plate (i.e. the perforation ratio r_p).

Moen and Schafer [3] established a prediction for the buckling of a rectangular plate with a large aspect ratio, and a single row of rectangular holes with a corner radius. They define two possible buckling modes; plate buckling away from the hole, or plate buckling of the unstiffened strip at the hole (or an interaction of the two) [3]. They consider buckling of the former type to be equal to the unperforated plate buckling load N_0, and buckling of the latter type (defined as USB in this paper) $N_{cr,USB}$ as follows (with variables described in Fig. 2):

$$N_{cr} = \min\left[N_0, N_{cr,USB}\right] \tag{4}$$

$$N_{cr,USB} = N_{cr,\mathrm{USB},net}\left(1 - \frac{l_y}{b}\right) \tag{5}$$

$$N_{cr,\mathrm{USB},net} = \min[N_{crA}, N_{crB}] \tag{6}$$

$$N_{cri} = k_i \frac{\pi^2 E}{12(1-\upsilon^2)}\left(\frac{t}{S_{yo,i}}\right)^2 \text{ (where } i = 1 \text{ or } 2) \tag{7}$$

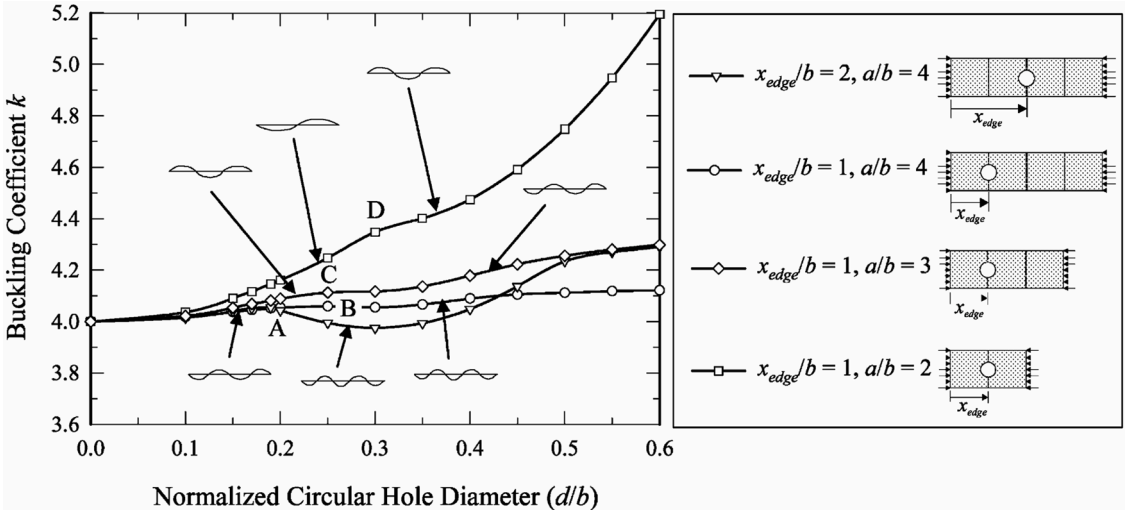

Fig. 5. Buckling coefficient (k) when the centre of a circular hole lies along the plate major axis and at a buckling minimum reproduced from [32].

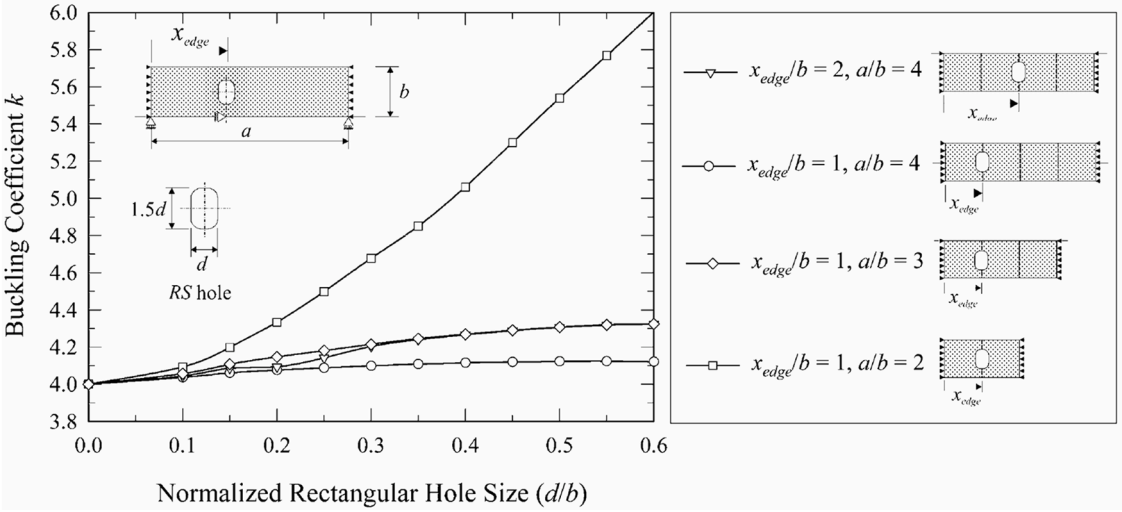

Fig. 6. Buckling coefficient (k) when the centre of a RH hole lies along the plate major axis and at a buckling minimum reproduced from [32].

$$\text{If } l_x \Big/ S_{yo,i} \geq 1; k_i = 0.425 + \frac{0.2}{\left(\frac{l_x}{S_{yo,i}}\right)^{0.95}} - 0.6 \tag{8}$$

$$\text{If } l_x / S_{yo,i} < 1; k_i = 0.925 \tag{9}$$

Some authors conduct experimental investigations on columns with a linear arrangement of perforations in their webs to suggest whether current design code predictions are appropriate, see [1,2,27–29]. Some of these studies have been used to inform modern standards (see Section 2.1).

2.3. Observations based on the literature

Minera et al. [22] determine that the introduction of a hole at the corners of a square plate is greatly weakening. For a square plate, the remainder of the sensitivity contour map somewhat mirrors the curvature of the buckled plate, i.e. the centre of the square plate has a greater curvature and thus is more sensitive to loss of stiffness [22]. However, as the aspect ratio of the plate becomes increasingly large, the plate centre is almost unaffected by stiffness change, rendering it more optimal to locate perforations here [22].

In agreement with [22,23] find that the centre of a square plate is vulnerable to the introduction of a hole. However, they find that the areas close to the centre of the plate edge are not equally sensitive to stiffness variation; a hole at the centre of the loaded edge can increase the plate buckling load whereas a similar hole at the centre of the unloaded edge cannot.

The findings of [13,30], and [31] seem to contradict the results found by [23] and [22]. Vann [30] and Sweedan and El-Sawy [13], determined that the influence of a circular hole on the elastic buckling load of a simply supported square plate is twofold. The first influence is a reduction to the plate bending stiffness in the portion of the plate where the hole is located; the second influence is a redistribution of stresses away from the centre of the plate and towards the supported edges [13, 30]. The former effect dominates for small holes, typically causing buckling load to reduce; the latter effect dominates for large holes, causing the buckling load to increase. As the hole diameter increases beyond 40–50 % of the plate width, the buckling load increases further – now the dominant factor is the redistribution of in-plane stresses to the sides [30,13].

Shakerley and Brown [31] make similar observations for the elastic buckling load of a simply supported square plate with a large concentric rectangular perforation. The buckling load can exceed that of an unperforated plate if the perforation is oriented with the major dimension perpendicular to the direction of compression (concentrating the compressive load into the two narrow strips above and below the hole). Such tall, narrow perforations (termed 'RH' perforations) are most beneficial; as the minor dimension of this perforation increases, the perforation tends towards an 'RL' hole where the major dimension is oriented parallel to the direction of compression. The aspect ratio of the remaining strips increases causing the buckling load to reduce [31].

However, this relationship is not observed by [32] who find that the elastic buckling load of a square plate always reduces with the diameter of a concentric circular hole (Fig. 3). Their observations are similar for plates of greater aspect ratio, when holes are located within the first half of an 'end panel', which provides the majority of the plate buckling resistance and are highly sensitive to stiffness variation (Fig. 4) [22,32]. If a hole is located at the buckling maximum within an 'end panel', a larger hole diameter causes a greater reduction to the elastic buckling load [33], similar behaviour is seen regardless of hole shape, orientation, or plate aspect ratio [32]. Yet, if a hole is located at the buckling maximum within an 'interior panel' (Fig. 4), the elastic buckling load may exceed the unperforated plate buckling load for large hole sizes [32, 33]. For a hole located at the buckling minimum (i.e. a 'nodal cross-line', Fig. 4), there may be a greater increase to elastic buckling load [32,33].

Depending on the length of the perforation, locating a hole at the buckling minimum causes little reduction in plate bending stiffness; therefore, the force redistribution effect is always dominant. Depending on the shape of the hole, the relationship between buckling coefficient and hole size for a plate of aspect ratio two is somewhat exponential,

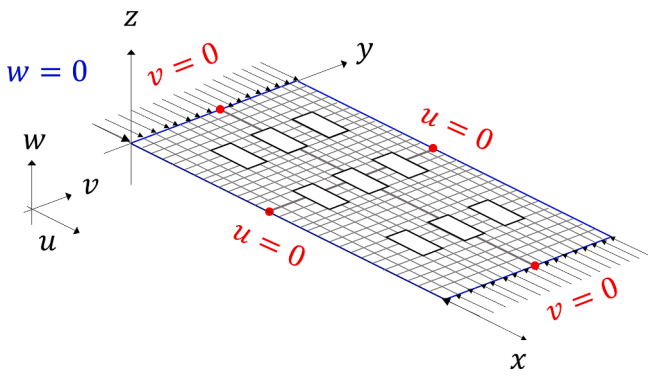

Fig. 7. Simply supported boundary conditions and nodal loading simulated in ABAQUS.

once the hole size exceeds a particular value (see Figs. 5 and 6, [32,33]).

When the hole height reaches this particular value, the number of buckling halfwaves increases or decreases, a phenomenon termed 'wavelength stiffening' (Fig. 5) as a change to the number of buckling halfwaves will increase the elastic buckling stiffness (provided that the hole is not too long) [3,13,32].

It has been shown that a plate with a central circular perforation of diameter equal to the width of a square perforation has a greater buckling load [5,34]. This is supported in an assessment on uniaxially compressed square plates undertaken by [35] and holds for eccentric perforations. Yu and Davis [34] attribute this to the difference in stress concentration, opposed to the difference in area of the two perforation shapes. Therefore, this research evaluates plates with an array of rectangular and square perforations and assumes that the latter is a conservative representation of a plate with circular perforations.

The relationship between the hole dimensions and buckling load also is somewhat dependant on the modeshape of the buckling plate. Plates with very small perforations exhibit Whole Plate Buckling (WPB) where the modeshape is little disturbed from the unperforated local buckling modeshape, accommodated by the network of remaining material [4,5].

The buckling modeshape changes for plates with larger perforations. For plates with a single row of closely-spaced perforations of any size, [13] and [29] found that the regions closer to the loaded edges (i.e. within the 'critical zone', Fig. 4) are most sensitive to buckling and exhibit the greatest out-of-plane displacement, and buckling is dampened at the holes. Small, closely spaced holes exhibit a reduction to elastic buckling load, whereas tall, closely spaced holes can lead to a buckling load greater than that of an unperforated plate, similar to the observations discussed for a plate with an RH hole [3].

For more widely spaced perforations there is less variation in stress. A single row of circular perforations exhibits a more uniform buckling modeshape [13]. However, the buckling modeshape of a plate with a single row of rectangular perforations is more complex. Buckling manifests at the sections transversely adjacent to a short rectangular hole, or at the sections laterally adjacent to a tall rectangular hole [3]. These are referred to as Unstiffened Strip Buckling (USB) and Lateral Perforation Buckling (LPB) respectively; LPB is indicative of 'wavelength stiffening' [3,4,13].

At particularly large hole spacings, the buckling load tends towards that of a plate with a single hole of the same dimensions [3,13]. Compared to plates with a single row of perforations, [4] found that plates with multiple rows in a grid-like arrangement exhibit a greater reduction to the elastic buckling load. They observe a fourth buckling mode between perforations, known as Euler Strip Buckling (ESB). The authors also determine that perforations closer to the longitudinal edges cause a larger loss in transverse membrane and bending stiffness.

3. Research objective and hypotheses

This research evaluates the buckling of plates with an array of rectangular and square perforations. The differential equation of the deflection surface is derived on the assumption of small deflections, and that the stress condition is constant throughout the plate, which is undergoing uniform bending [36]. According to this theory, the bending stresses within a buckling plate of uniform thickness and material properties are a function of the deflection function $w = f(x,y)$:

$$\frac{\partial^4 w}{\partial x^4} + 2\frac{\partial^4 w}{\partial x^2 \partial y^2} + \frac{\partial^4 w}{\partial y^4} = \frac{p(x,y)}{D} \tag{10}$$

When holes are introduced into the plate, the bending stress now depends on a superposition of curvature and the equilibrating moment at the hole periphery [36]. Therefore, the Kármán-Föppl equations for a variable stress field should be considered (written in terms of the Airy stress function ϕ, and where q represents any out of plane loading [37]):

$$\begin{aligned}\nabla^4\phi &= Et\left(\frac{\partial^2 w}{\partial x \partial y} - \frac{\partial^2 w}{\partial x^2}\cdot\frac{\partial^2 w}{\partial y^2}\right) D\left(\frac{\partial^4 w}{\partial x^4} + 2\frac{\partial^4 w}{\partial x^2 \partial y^2} + \frac{\partial^4 w}{\partial y^4}\right) \\ &= q + \left(\frac{\partial^2 \phi}{\partial y^2}\cdot\frac{\partial^2 w}{\partial x^2} + \frac{\partial^2 \phi}{\partial x^2}\cdot\frac{\partial^2 w}{\partial y^2} - 2\frac{\partial^2 \phi}{\partial x \partial y}\cdot\frac{\partial^2 w}{\partial x \partial y}\right)\end{aligned} \tag{11}$$

However, as the number and size of perforations increase, the stress state becomes incredibly complex. This causes localised variations in the deflection function w (as the curvature and bending stresses are coupled), such that the linearised expressions for the curvature are invalidated. Thus, a theoretically-derived solution for the elastic buckling load may be impossible to find, albeit incredibly computationally demanding. This necessitates the development of empirical expressions for the elastic buckling load, which is the research objective of this paper.

This superposition of stress states is used to frame a hypothesis for the relationship between the elastic buckling load and the height of the perforations. For particularly small perforations, the influence on the bending stress state is negligible, Eq. (10) is reasonably valid, and the elastic buckling load will tend towards that of the unperforated counterpart.

However, for a small-medium sized hole located near the plate centre, the superposition of stresses occurs at the most onerous location, as the hole border is located at an area of greater curvature. This may be why the elastic buckling load reduces when a small hole is located at the buckling maximum [22,23]. Conversely, the effect is stabilising for a tall concentric hole, as the superposition occurs in a region of smaller curvature, and stresses are diverted to the supports. It is hypothesised that tall perforations will enable the greatest increase to the elastic buckling load.

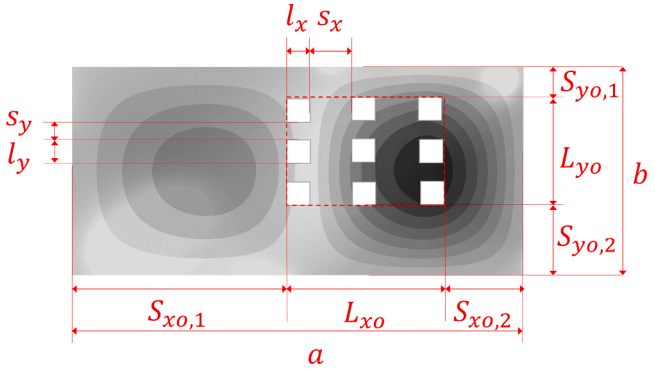

Fig. 8. Regular variables examined.

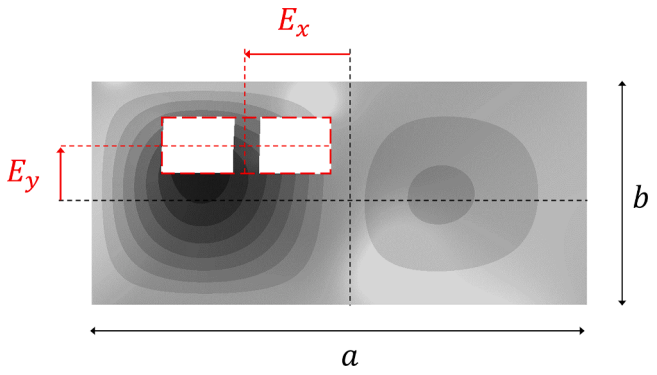

Fig. 9. Eccentricity.

4. Finite element model

To determine the nature of the relationship between the critical elastic buckling load of a perforated simply supported thin plate and the parameters discussed, performance is investigated with the finite

Table 1
Domain of variables examined in parametric study.

	a_r	b/t	n_r	n_c	S_{xo}/a	S_{yo}/b	L_{xo}/a	L_{yo}/b	s_x/a	s_y/b	l_x/a	l_y/b	e_x	e_y
Mean	2.62	100	2.00	9.00	0.163	0.183	0.495	0.426	0.060	0.252	0.051	0.210	0.089	0.104
Minimum	1.00	100	1.00	2.00	0.045	0.040	0.032	0.047	0.005	0.015	0.004	0.020	0	0
Maximum	5.32	100	5.00	30.0	0.410	0.461	0.907	0.890	0.710	0.890	0.347	0.890	0.360	0.380

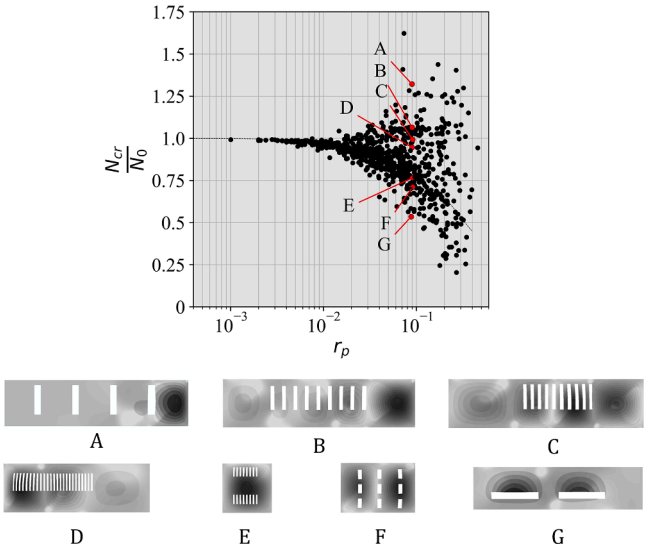

Fig. 10. The load ratio of the perforated plate to the unperforated plate with respect to perforation ratio for all 870 parametric models.

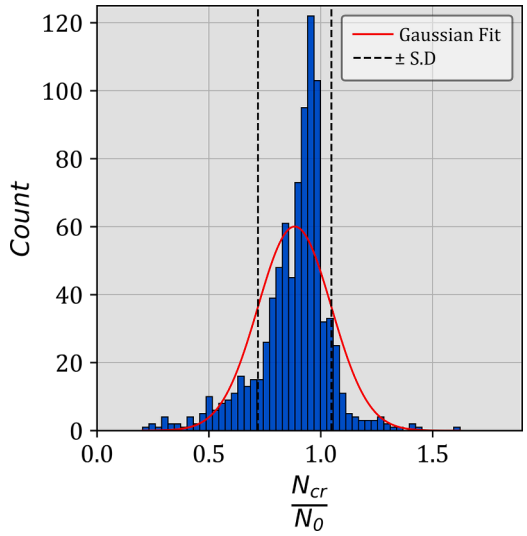

Fig. 11. Distribution of load ratio for all 870 models in the dataset.

element (FE) method. This is determined with the ABAQUS linear perturbation procedure [38], which solves the eigenvalue problem of the constitutive and geometric stiffness matrices.

The material is steel with a Young's Modulus of 203.4 GPa, and a Poisson's ratio of 0.3. It is assumed to have isotropic properties and obey the stress-strain relationships for isotropic materials. The perforated plate buckles in the elastic regime, with slenderness determined in accordance with [26] and [39]. The following limit ensures the plate is slender for all variables investigated in terms of the plate width (b) and thickness (t):

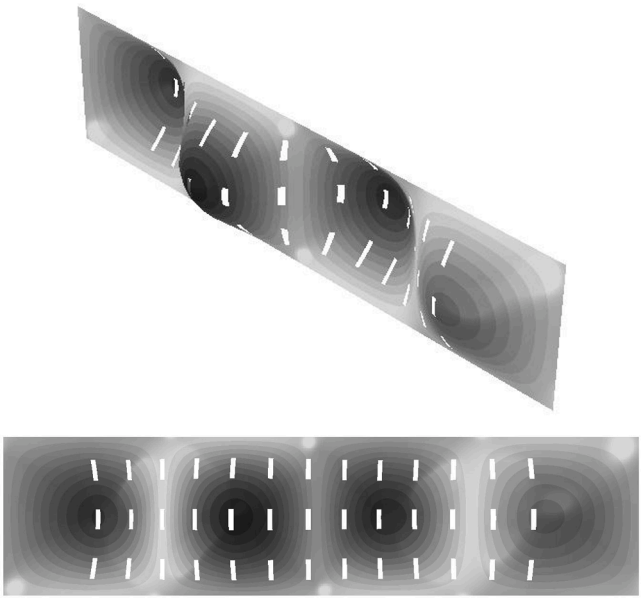

Fig. 12. WPB involves the net plate area.

$$\min\left(\frac{b}{t}\right) = 100 \tag{12}$$

As the plate thickness is very small in comparison to the plate dimensions, the problem is adequately described by Kirchhoff's shell theory, and thin shell quadratic elements with reduced integration (S8R5) are chosen. A structured mesh is used to negate transverse shear locking and allow for easier data management and thus faster convergence.

All perforations are oriented with their major and minor dimensions parallel to the axes of the global co-ordinate plane, which allows for rectangular FE elements everywhere. A limit is placed on the aspect ratio of elements in the mesh to further ensure accurate convergence, according to an investigation by [40].

$$\min\left(\frac{a_e}{b_e}\right) = 1,\ \max\left(\frac{a_e}{b_e}\right) = 1.5 \tag{13}$$

where a_e and b_e represent the length and width of the finite element respectively. Simply supported boundary conditions are represented as shown in Fig. 7. This is similar to the conditions applied by [13] who examine a symmetrical distribution of circular perforations arranged along the length. Compressive uniform edge loading is simulated by consistent nodal loads, as considered by [24]. ABAQUS input files are generated with a custom-built python script where these meshing, loading and boundary conditions are prescribed to the model.

The FE model has been used to reproduce the results produced by [24] who examined 32 FE models of plates with rectangular holes with a corner radius. Despite the holes in this study being sharp-cornered, the results accurately follow the same trend. The limit on the maximum element size is chosen as a consequence of this comparison, defined as:

$$\max\left(\frac{b_e}{b}\right) = 0.02 \tag{14}$$

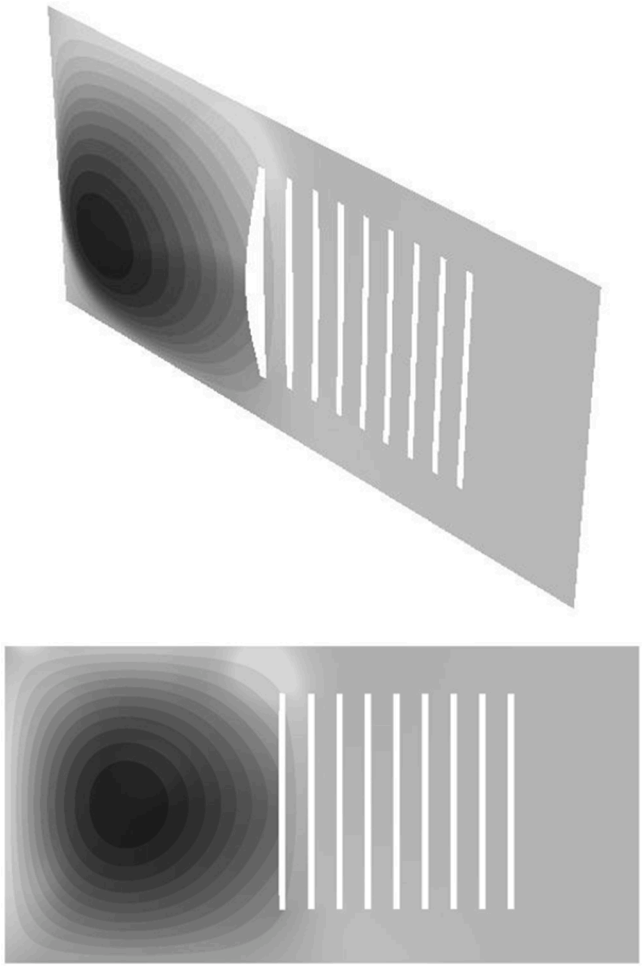

Fig. 13. LPB at the lateral portion between the perforation and plate edge.

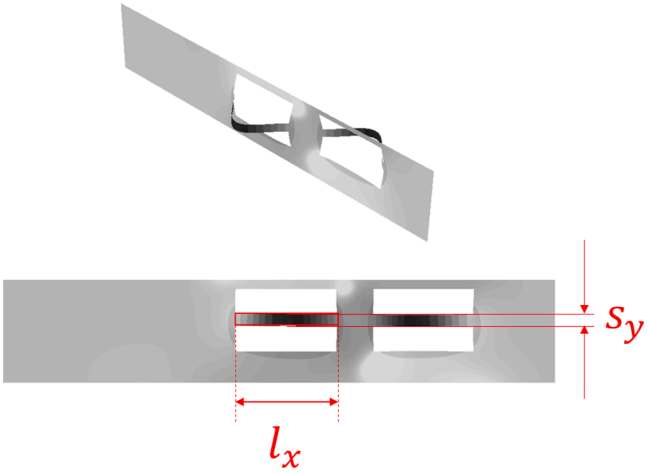

Fig. 14. ESB at the transverse portions between perforations.

4.1. Parametric assessment

The parametric analysis follows [25]. Rectangular holes perforate a defined region with dimensions L_{xo} and L_{yo} (Fig. 8), and perforations are arranged in rows and columns (with the number n_r and n_c respectively) at some eccentricity about the plate centroid. The x- and y- eccentricity (e_x, e_y respectively) is defined as the ratio of the average centroid (E_x, E_y respectively, Fig. 9) to the plate width (b) and length (a) respectively. Distances from this region to the edges are denoted $S_{xo,i}$ and $S_{yo,i}$ (Fig. 8), with S_{xo} and S_{yo} being the smaller distance (Table 1). Fig. 8 also defines the perforation spacing and size. The perforation ratio r_p is the ratio of total hole area to the gross plate area. The aspect ratio a/b is denoted as a_r.

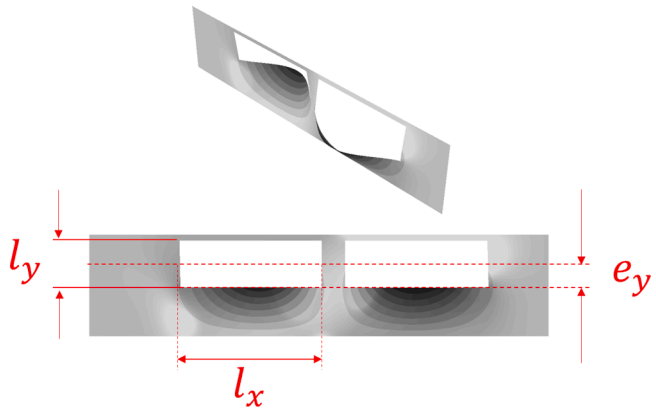

Fig. 15. USB at the transverse portion between the perforation and plate edge.

A total of 870 parametric models with regularly spaced perforations has been generated such that the variables are randomly selected from the domain using the python 'randrange' function [41], and the elastic buckling load is determined by FE analysis with ABAQUS. For each of these models, the ratio of the perforated plate buckling load (N_{cr}) to the unperforated plate buckling load (N_0) (termed the 'load ratio') is plotted with respect to the perforation ratio (r_p) (Fig. 10). It ranges from 0.204 to 1.62 with considerable scatter. A Gaussian distribution of these results is shown for a histogram of the results with 50 bins, in (Fig. 11); the standard deviation (S.D) of ± 0.164 is shown by the dotted lines. Of these 870 models, 14.8 % have a load ratio greater than one, and thus exhibit an increased elastic buckling load when perforated to when unperforated.

Although the points highlighted correspond to a similar perforation ratio r_p, the buckling mode and buckling load varies considerably (Fig. 10). Example A exhibits LPB, and the greatest increase to the buckling load (Fig. 10), whereas G exhibits USB, and the greatest reduction to the buckling load. The buckling modeshape of example E and F exhibit a strong resemblance to the unperforated plate, demonstrating WPB. As the wavelength and amplitude of the buckles in B and C exhibit small variation throughout the plate, examples B and C are considered as "weakly WPB". Such behaviour is on the border of what is termed an 'interaction' (INT) of buckling modes (in this case a WPB-LPB interaction); example D does not portray a strong resemblance to any of the four buckling types and is classified as such. For the r_p selected, none of the models exhibits ESB, and examples are given in the following section. As a plate with a given perforation ratio can exhibit a range of buckling modes, it follows that empirical equations for the elastic buckling loads must be established with alternative variables.

5. Local Bukcling mode algorithm

A perforated plate exhibiting Whole Plate Buckling (WPB) shows very little difference in modeshape to its unperforated counterpart (Fig. 12). This is typical where the influence of perforations on the stress field is quite small. In comparison to an unperforated plate, a plate with a random distribution of perforations exhibiting Whole Plate Buckling (WPB) typically exhibits a reduced elastic buckling; primarily because the perforations are quite small, so the reduction to the plate bending stiffness dominates over the beneficial effect of stress redirection to the supported edges (Section 3).

A perforated plate exhibits little difference in behaviour to an

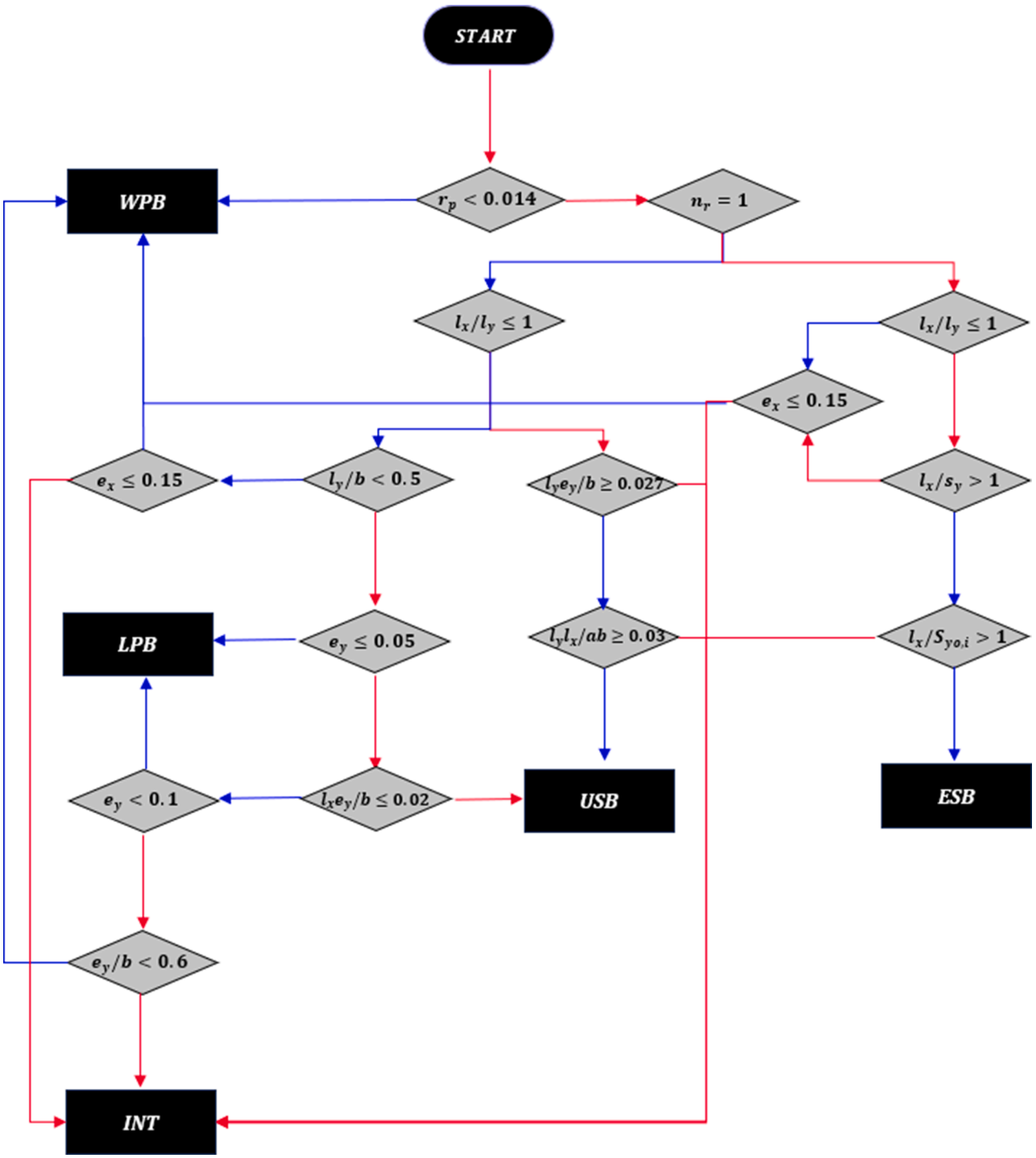

Fig. 16. The algorithm used to determine the buckling mode corresponding to the geometry of a plate with an array of rectangular perforations. 'Yes' and 'No' are blue and red respectively.

equivalent unperforated plate when the total perforated area is particularly small, this limit is approximately $r_p = 0.014$ (Fig. 10) and therefore must exhibit WPB by definition. If $a_r > 1$, the WPB mode will interact with USB or ESB, as the increase in the aspect ratio of areas above and below the perforation causes a localised unstiffened plate behaviour. If, however, the aspect ratio of the perforation is less than one, with a particularly large height ratio, the WPB mode may interact with LPB, as the beneficial effect of stress redirection to the supported edges becomes dominant. This effect also dominates if the average eccentricity of the perforations is particularly large. The WPB buckling load of a plate is particularly sensitive to e_x, as the plate behaviour greatly depends on how far perforations exceed into the 'end panel' (Fig. 4). If $e_x < 0.15$, a plate will buckle by WPB without interacting with any other modes (Fig. 12).

Of the four buckling modes, a plate undergoing LPB is more likely to exhibit an increase in elastic buckling load to the unperforated state. LPB is typical of plates with one row of particularly tall perforations ($l_y > 0.6b$), with $e_y < 0.1$ to negate interaction with other modes (Fig. 13). USB may occur instead of LPB, depending on the aspect ratio of the portion above and below the perforation which can be summarised

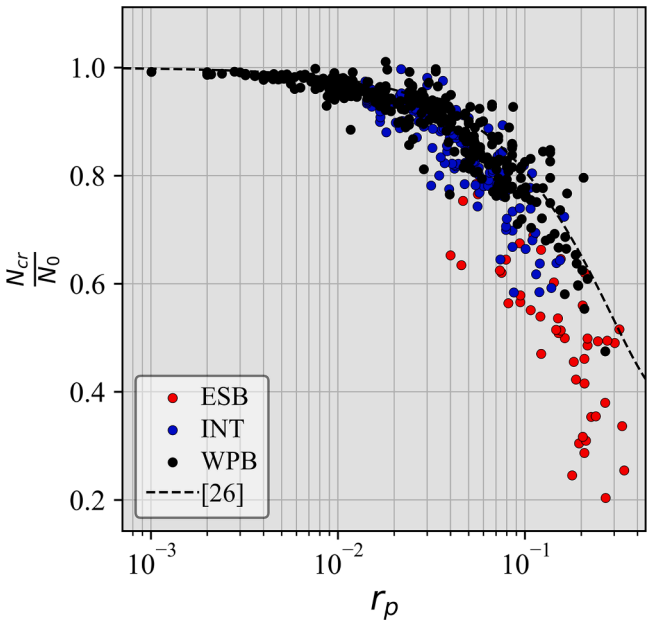

Fig. 17. Relationship between elastic buckling load ratio and perforation ratio for plates with $n_r > 1$.

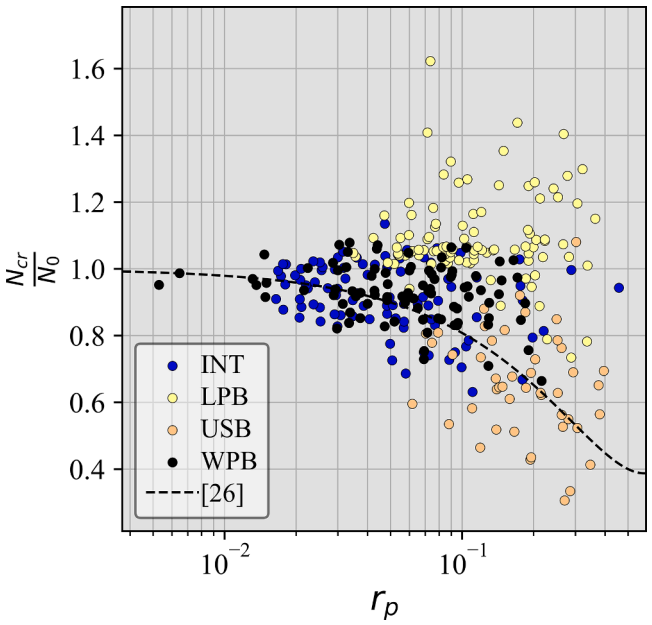

Fig. 18. Relationship between elastic buckling load ratio and perforation ratio for plates with $n_r = 1$.

by the ratio $l_x e_y/b$. Interaction with the WPB mode dominates for a row of holes with $0.5b < l_y < 0.6b$, and $e_y \geq 0.1$. There is a redistribution of forces to the plate edges, and the portions between the hole and the plate edge undergo a great increase in stiffness due to the greater force concentration, resulting in a pinning behaviour. Buckling is 'pushed' into the sections laterally adjacent to the perforations.

ESB is best described as column-like plate behaviour (Fig. 14). For it to happen, there must be $n_r > 1$ and $l_x/s_y > 1$. However, there will be an ESB-USB interaction if $l_x/S_{y0} > 1$. USB is akin to localised unstiffened plate behaviour, typical of plates with a single row of large perforations (Fig. 15). It manifests when $S_{y0,i}$ is particularly large; however, this variable cannot adequately describe USB behaviour which is highly sensitive to e_y. For example, a concentric line of perforations may

Table 2
Functions $f(X)$ and $g(x_i)$where i takes values from 1 to n for plates with $n_r > 1$.

Option	$f(X)$	$g(x_i)$	*n*
0	$1.8X^2 - 2.1X + 1$	r_p	1
1	$e^{-3.16X}$	r_p	1
2	$e^{-1.15X}$	$r_p \cdot \frac{a}{b}$	3
3	$e^{-4.96X}$	$r_p \cdot \left(0.287\frac{S_{yo}}{b} + 0.594\frac{l_y}{b} + 1.52\frac{l_x}{a} + 0.0802\frac{a}{b} + 1.73E_x + 0.718E_y\right)$	8
4	$e^{-1.96X}$	$r_p \cdot \left(\left(\frac{S_{yo}}{b}\right)^{5.04} + \left(\frac{l_y}{b}\right)^{3.43} + \left(\frac{l_x}{a}\right)^{0.546} + \left(\frac{a}{b}\right)^{0.140} + E_x^{0.440} + E_y^{1.71}\right)$	8
5	$e^{-0.714X}$	$r_p \cdot \left(\left(\frac{S_{yo}}{b}\right)^{-0.407} + \left(\frac{l_y}{b}\right)^{-0.274} + \left(\frac{l_x}{a}\right)^{0.452}\right)$	6
6	$e^{-2.04X}$	$r_p \cdot \left(\left(\frac{a}{b}\right)^{0.230} + E_x^{0.360} + E_y^{1.33}\right)$	5

Table 3
R^2 test performance for plates with $n_r > 1$, assessed for n models in each mode.

Option n	R^2 543	R^2_{WPB} 360	R^2_{INT} 135	R^2_{ESB} 48
[3]	-1.69	-3.96	-2.95	-8.30
[4]	0.416	0.607	0.023	-3.32
0 [26]	0.711	0.848	0.523	-1.31
1	0.822	0.734	0.724	0.071
2	0.719	0.452	0.210	0.313
3	0.877	0.767	0.768	0.539
4	0.880	0.815	0.781	0.429
5	0.871	0.843	0.852	0.193
6	0.861	0.785	0.730	0.356

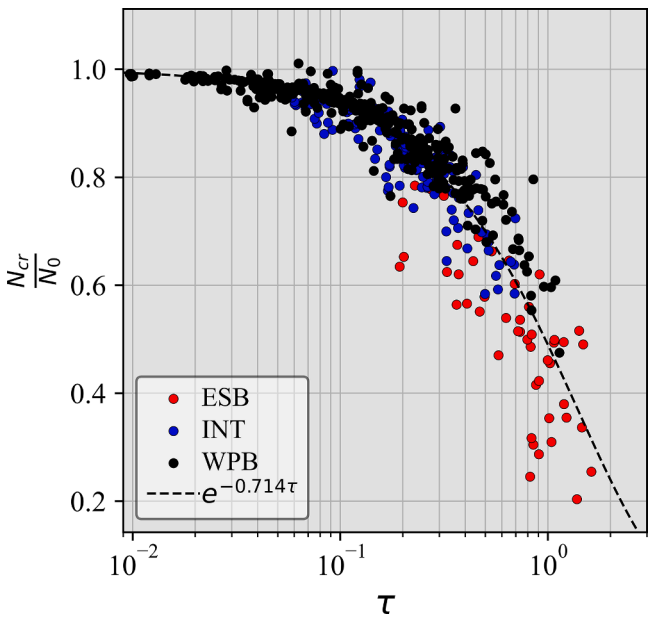

Fig. 19. Relationship between the load ratio and τ for plates with $n_r > 1$.

possess a large $S_{y0,i}$ but is more likely to exhibit WPB or a WPB-USB interaction. The condition $l_y e_y/b \geq 0.027$ encapsulates these behaviours.

Although USB is typical when $l_x/l_y \geq 1$, it can occur instead of LPB for perforations with $l_x/l_y > 1$ as described. In comparison to an unperforated plate, the former case causes a reduction in elastic buck-

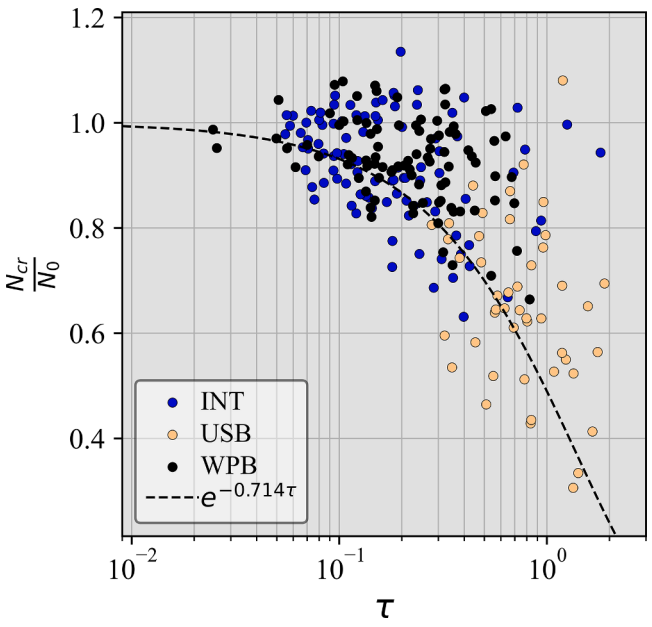

Fig. 20. Relationship between load ratio and τ for plates exhibiting WPB, INT or USB with $n_r = 1$.

ling load, whereas the latter case may enable it to increase. Therefore, the limits for the USB domain are much more complex than other local perforated plate buckling modes.

The numerical limits given for the various conditions discussed were determined iteratively. For example, the limit $l_y e_y/b$ was varied between 0.025 and 0.035 for a collection of models, which were sorted into one of the five mode subsets. The final limit of 0.027 optimised the number of correctly identified deformation modes, while minimising the number of incorrectly identified models. This process determined numerical limits on a plate's dimensions, establishing an algorithm to identify local plate buckling modes.

The performance of the resulting algorithm shown in Fig. 16 was compared to a logistic regression model developed with machine learning using python's scikit-learn module [42]. To mitigate training

Table 4
Functions $f(X)$ and $g(x_i)$ where i takes values from 1 to n for plates with $n_r = 1$.

Option	$y = f(X)$	$X = g(x_i)$	*n*
0	$1.8X^2 - 2.1X + 1$	r_p	1
1	$e^{-1.48X}$	r_p	1
2	$0.740 + X$	$0.0199m - 0.123E_x - 0.567E_y + 0.129\left(\frac{S_{xo,2}}{a}\right) + 0.317\left(\frac{S_{yo,1}}{b}\right) + 0.298\left(\frac{S_{yo,2}}{b}\right) + 0.333\left(\frac{s_x}{a}\right) + 0.125\left(\frac{s_y}{b}\right) + 0.125\left(\frac{L_{yo}}{b}\right) - 1.50\left(\frac{l_x}{a}\right) + 0.125\left(\frac{l_y}{b}\right)$	13
3	$e^{-0.0391X}$	$0.407m - 5.28E_x + 17.5E_y - 10.3\left(\frac{S_{xo}}{a}\right) + 1.22\left(\frac{S_{yo}}{b}\right) - 12.0\left(\frac{s_x}{a}\right) - 0.549\left(\frac{s_y}{b}\right) - 0.549\left(\frac{L_{yo}}{b}\right) + 46.4\left(\frac{l_x}{a}\right) - 0.549\left(\frac{l_y}{b}\right)$	12
4	e^{X}	$(0.463E_x + 1.31E_y)\cdot\left(-9.12\frac{l_x}{a}\right)$	4
5	$e^{-20.4X}$	$(0.146E_x + 0.489E_y)\cdot\left(\left(\frac{l_x}{a}\right)^{0.891} + \left(\frac{l_y}{b}\right)^{22.0}\right)$	6
6	$e^{-1.58X}$	$\left(\left(E_x + \frac{l_y}{b}\right)^{35.3} + \left((E_y)^{1.08} + \left(\frac{l_x}{a}\right)^{0.561}\right)\right)^{2.28}$	**6**

Table 5
R^2 test performance for plates with $n_r = 1$, assessed for each mode.

Option n	R^2 232	R^2_{WPB} 91	R^2_{INT} 95	R^2_{USB} 46
[3]	-1.79	-9.57	-5.82	-0.158
[4]	0.185	-0.327	-0.355	-0.945
0 [26]	0.223	-0.797	-0.681	-0.207
1	0.311	-0.260	-0.241	-0.489
2	0.790	0.474	0.609	0.649
3	0.791	0.569	0.626	0.576
4	0.708	0.198	0.527	0.498
5	0.711	0.248	0.513	0.494
6	0.766	0.515	0.592	0.514

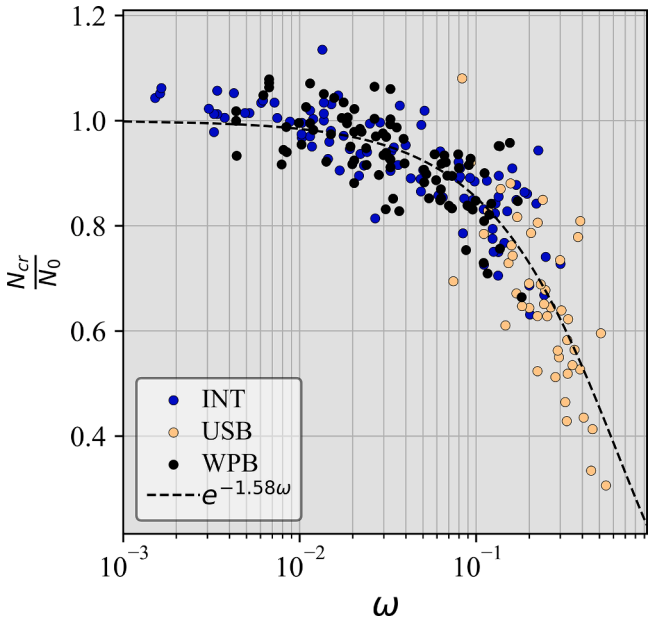

Fig. 21. Relationship between the load ratio and ω for plates exhibiting WPB, INT or USB with $n_r = 1$.

on a large proportion of incorrectly classified plates, this model was trained on half of all 870 results determined with the algorithm. The random seed (i.e. collection of results used to train the model) was changed 50 times and the predictions for the test set were output each of the 50 times. Then the predicted result was compared to the 'true' result determined with the algorithm (Fig. 16). A given result will therefore have x number of predictions based on the collection of test sets it appears in. If the elastic buckling mode predicted with the algorithm disagrees to the mode predicted with logistic regression for >25 % of these x results, then it is assumed that the model was miss-classified with the algorithm. By this assessment, only 2.76 % of all parametric results were miss-classified, i.e. the algorithm is very good at identifying the correct mode.

6. New prediction method

When the algorithm is applied to the dataset of 870 models, the number of models identified for the WPB, ESB, USB, and LPB subsets are 451, 48, 46 and 95 respectively; the remaining 230 models exhibit an interaction (INT) of at least two modes. The prediction developed by [26] depends solely on the unperforated plate buckling load N_0 and the perforation ratio r_p. However, we can observe that the relationship between the elastic buckling load ratio (N_{cr}/N_0) and r_p is starkly different for plates with $n_r > 1$ (Fig. 17) compared to that for plates with $n_r = 1$ (Fig. 18). In particular, plates with $n_r > 1$ with ESB deformation, and plates with $n_r = 1$ with LPB deformation, possess a greater deviation

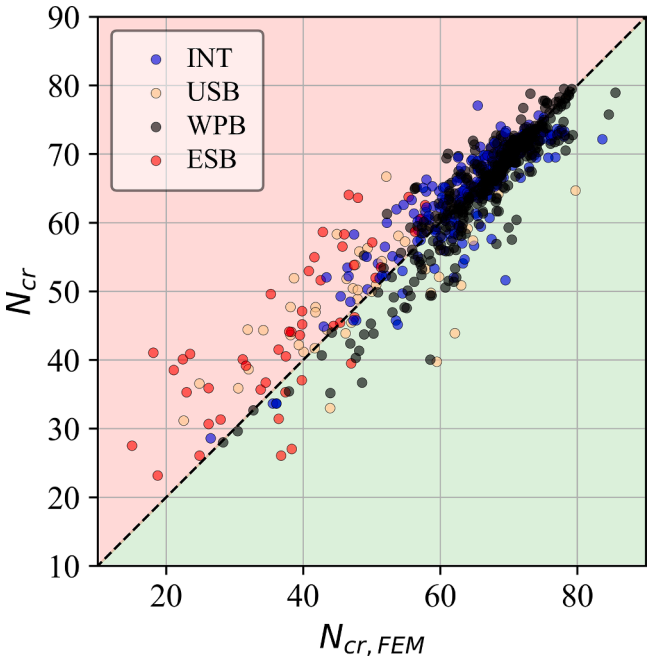

Fig. 22. Relationship between predicted (N_{cr}) and FE ($N_{cr,FEM}$) elastic buckling loads for all 775 considered geometries, including WPB, ESB, USB, INT, excluding LPB. Points in the green region are conservative.

from the general trend with respect to r_p.

These observations directed a study to establish empirical predictions for the elastic buckling load ratio $Y = N_{cr}/N_0$ as a function $Y = f(X)$, where $X = g(x_i)$, expressed in terms of dimensionless parameters x_i, These parameters are related to the geometry of the perforations within the plate, summarised in Figs. 8 and 9.

The method to establish the dominant parameters and numerical coefficients followed a hybrid approach termed 'machine-learning-directed-regression-analysis'. In this approach, machine learning was used for feature selection (i.e. to identify the dominant variables x_i at the 5 % significance level) while regression analysis was used to fit a custom functional form of the equation (i.e. $X = g(x_i)$). As the elastic buckling load ratio depends on whether the number of rows of perforations is equal to or greater than one, a prediction is established for each of these subsets. The functions $g(x_i)$ are τ and ω for plates with $n_r > 1$ and $n_r = 1$ respectively.

The chosen expression must meet three objectives. Firstly, it must be accurate for the 'target' subset of plates, defined in the next sections. Secondly, it must be accurate for a distinct mode, identified with the algorithm. This 'accuracy' is determined by the R^2 test result, which is used to evaluate how well the proposed regression model fits the data. The third objective is that it must be simple; it is desired to minimise the number n of constants and variables x_i where i varies from 1 to n. The scipy.optimize.minimize function [43] was used to determine the coefficients a_i with least squares regression.

6.1. An expression for plates with $n_r > 1$

In this subset, 360 and 48 models are identified to exhibit WPB and ESB respectively; the remaining 135 models exhibit an interaction (INT) of at least two modes. It was discussed that ESB demonstrates a greater deviation from the general trend with respect to r_p than WPB and INTeraction modes for plates with $n_r > 1$. Regardless, it will be shown that the proposed variable τ can be used to establish the elastic buckling load ratio for all plates with $n_r > 1$, and thus the target subset. Machine learning was not necessary for these plates, as r_p already provides a very good starting point for the choice of dominant variables (Fig. 17).

A series of potential equations were used to predict the elastic buckling load of plates with more than one row of perforations. The proposed options for $f(X)$ and $g(x_i)$ are shown in Table 2, and determined by iteratively modifying $g(x_i)$ according to the observed performance. This performance is described by the R^2 test result, given for each option and mode in Table 3. Note that the results are determined for non-rounded coefficients a_i, which are given in Table 2 to three significant figures. The expression proposed by [26] is given in the first row of Table 2, and the performance is given in Table 3, in addition to that of the predictions by [3] and [4].

All of the proposed options exceed the performance of the prediction proposed by [3,26] and [4] for the entire target subset. This is unanticipated given that the parametric domain examined by [4] is similar to

Table 7
The factor γ determined for each mode with n models at the 5 % and 1 % significance level.

Mode	n	$\gamma_{5\%}$	$\gamma_{1\%}$
WPB	451	1.06	1.15
INT	230	1.12	1.18
USB	46	1.38	1.47
ESB	48	1.83	2.27
$n_r > 1$	543	1.15	1.54
$n_r = 1$ (*not LPB*)	232	1.17	1.38
All (*not LPB*)	775	1.17	1.41

Table 6
Mean (μ), COV and R^2 test performance for the elastic buckling load of a perforated plate found with FEM to that found with various methods, for different subsets of n parametric models.

		$n_r > 1$			$n_r = 1$		
Modes		WPB, INT, ESB	WPB, INT	ESB	WPB, INT, USB	WPB, INT	USB
n		543	495	48	232	186	46
[3]	μ	1.06	1.107	0.568	1.38	1.40	1.28
	COV	0.406	0.377	0.306	0.303	0.318	0.196
	R^2	-1.69	-3.27	-8.30	-1.79	-7.39	-0.158
[4]	μ	0.913	0.938	0.654	0.984	1.02	0.854
	COV	0.122	0.065	0.254	0.18	0.139	0.280
	R^2	0.416	0.470	-3.22	0.185	-0.336	-0.945
[26]	μ	0.945	0.967	0.716	1.06	1.07	1.00
	COV	0.104	0.054	0.208	0.186	0.154	0.283
	R^2	0.711	0.766	-1.31	0.223	-0.721	-0.207
Eq. (16)	μ	1.00	1.01	0.870	**N/A**		
	COV	0.088	0.056	0.219			
	R^2	0.871	0.858	0.193			
Eq. (19)	μ	**N/A**			1.00	1.01	0.976
	COV				0.102	0.072	0.179
	R^2				0.765	0.562	0.514

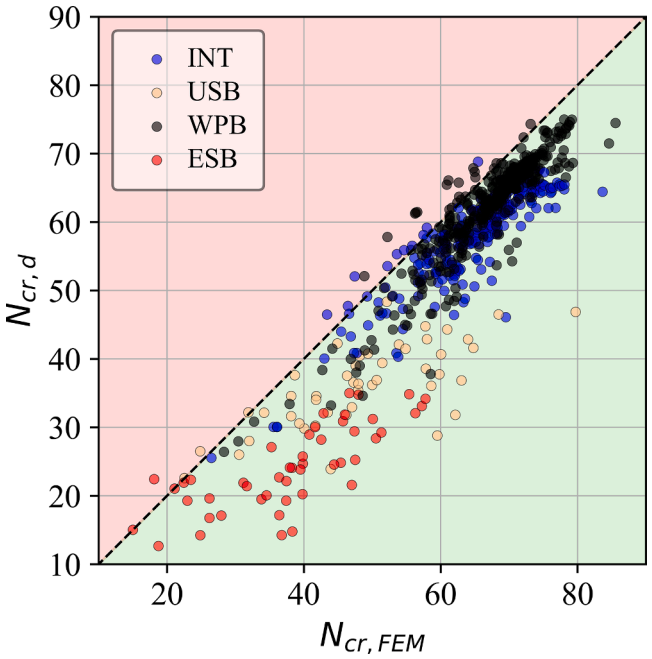

Fig. 23. Relationship between predicted ($N_{cr,d}$) and FE ($N_{cr,FEM}$) elastic buckling loads for all 775 considered geometries, including WPB, ESB, USB, INT, excluding LPB. Points in the green region are conservative.

that examined here (Table 1). Option 5 is assessed to best meet each of the desired objectives. Therefore, the elastic buckling load of plates with $n_r > 1$ is found with the following equation, where variables are defined in Fig. 8:

$$\tau = r_p \cdot \left(\left(\frac{S_{yo}}{b}\right)^{-0.407} + \left(\frac{l_y}{b}\right)^{-0.274} + \left(\frac{l_x}{a}\right)^{0.452} \right) \tag{15}$$

$$N_{cr,n_r>1} = N_0 e^{(-0.714\tau)} \tag{16}$$

The elastic buckling load determined with Eq. (16) for plates with $n_r > 1$ is plotted with respect to the variable τ in Fig. 19.

Table 3 also provides the R^2 test result for plates exhibiting ESB which is found to be particularly poor. ESB behaviour is characterised by local buckling at the portion of the plate between perforations. Thus, assuming that $l_x \gg s_y$ and that the full length l_x is effective, one can posit that $N_{cr,ESB}$ per unit width could be approximated as:

$$N_{cr,ESB} = \frac{\pi^2 E}{l_x^2} \cdot \frac{t^3}{12} \cdot \frac{(b - l_y n_r)}{b} \tag{17}$$

However, when used to determine the elastic buckling load ratio, an R^2 test score of -40.8 is obtained for Eq. (17) i.e. inferior to the score determined with the new expression proposed in Eq. (16). It follows that Eq. (16) should be used to determine $N_{cr,ESB}$, despite the fact that the R^2 test result for plates exhibiting ESB is much poorer than WPB and INTeraction modes.

6.2. An expression for plates with $n_r = 1$

In this subset, the number of models identified for the WPB, USB, LPB, subsets are 91, 46 and 95 respectively; the remaining 95 models exhibit an interaction (INT) of at least two modes. On observation and mathematical analysis, plates with $n_r = 1$ deforming by LPB exhibit a separate behaviour to that of other buckling modes with $n_r = 1$. Therefore, only plates with $n_r = 1$ exhibiting WPB, USB or an INTeraction of modes define the target subset and are used to develop an expression for the elastic buckling load. The subset of plates with $n_r = 1$ exhibits a very poor relationship with the perforation ratio r_p (Fig. 18) and τ (Fig. 20). When [26] and Eq. (16) are used to determine the elastic buckling capacity ratio for this subset, the R^2 test score is 0.223 and -1.22 respectively.

To establish a new initial function f(X), machine learning was used again to determine the dominant variables. Backwards elimination was performed to build a multivariable linear regression model. The following procedure to determine functions f(X) and $g(x_i)$ was performed iteratively by regression analysis, and by addressing the performance of the corresponding equation with the R^2 test. The proposed options are summarised in Table 4, their performance evaluations are given in Table 5, and the relationship with the chosen variable ω is shown in Fig. 21.

Option 6 requires half the number of the variables n considered in the expressions determined with machine learning, with only a 6.58 % lower performance score. It predicts the elastic buckling load ratio for plates with $n_r = 1$ as follows:

$$\omega = \left(\left(E_x + \frac{l_y}{b} \right)^{35.3} + \left((E_y)^{1.08} + \left(\frac{l_x}{a}\right)^{0.561} \right) \right)^{2.28} \tag{18}$$

$$N_{cr,n_r=1} = N_0 e^{(-1.58\omega)} \tag{19}$$

7. Predicting formulae for N_{cr}

In summary, two new equations are proposed: Eq. (16) for plates with $n_r > 1$ and Eq. (19) for plates with $n_r = 1$ with the exclusion of LPB. Finally, the evaluated elastic buckling loads (N_{cr}) are plotted against the numerically computed buckling load with FE analysis ($N_{cr,FEM}$) in Fig. 22 for all 775 models (i.e. excluding LPB models). We find a mean accuracy and COV of 1.00 and 0.093 respectively, and an overall R^2 coefficient of 0.840. The proposed Eqs. (16) and (19) exhibit the best performance for each of the subsets examined in Table 6, where performance is defined by the best R^2 test result. However, the performance of the ESB subset is very poor.

The models in the ESB and USB subsets have a mean ratio less than unity, and are thus unconservatively approximated. In line with Eurocode, the design elastic buckling load is defined as:

$$N_{cr,d} = \frac{N_{cr}}{\gamma} \tag{20}$$

This is a lower bound approach, where the statistical model factor γ is chosen to ensure that the probability of unconservative design is limited to only α% of cases, such that:

$$P\left(N_{cr,FEM} \geq N_{cr,d}\right) = 1 - \alpha \tag{21}$$

To ensure that the actual buckling resistance determined with FE analysis ($N_{cr,FEM}$) exceeds the design value ($N_{cr,d}$) with at least a 95 % probability, the model factor is found for $\alpha = 0.05$ ($\gamma_{5\%}$). It is also found for $\alpha = 0.01$ ($\gamma_{1\%}$), for a probability that 99 % of predictions will be less than the actual buckling resistance. The value for γ is given in Table 7 for each local plate buckling mode. The results are displayed in Fig. 23 for all 775 models, such that $\gamma_{WPB,5\%} = 1.06$ is applied for all 451 WPB models, $\gamma_{INT,5\%} = 1.12$ is applied for all 230 INT models, $\gamma_{USB,5\%} = 1.38$ is applied for all 46 models, and $\gamma_{ESB,5\%} = 1.83$ is applied for all 48 ESB models.

8. Conclusions

This research investigates the elastic buckling behaviour of rectangular plates with a regular array of perforations. The local buckling of such plates can exhibit one of four modes: Whole Plate Buckling (WPB), Euler Strip Buckling (ESB), Unstiffened Strip Buckling (USB), Lateral Perforation Buckling (LPB) or an interaction (INT) of them. A parametric study of 870 models is first conducted to develop an algorithm for determining the buckling mode based on plate and perforation

dimensions. We demonstrate that this algorithm can be reliably used to determine which of the four types of mode will dominate. At the extents of each of the four domains, interaction occurs (INT), and a particular mode is visually 'weaker'.

Of the models examined in this study, a plate with one row of perforations exhibiting LPB possess the greatest average l_y/b, with a mean increase to the elastic buckling load of the unperforated plate counterpart of 12 %. In comparison, plates with one row of perforations exhibiting WPB or USB exhibit a mean reduction to the elastic buckling capacity of the equivalent unperforated plate of 7 % and 34 % respectively. Plates with a regular array of square or rectangular perforations with more than one row exhibit an even greater reduction to the unperforated plate elastic buckling capacity, of 10 % and 49 % for WPB and ESB respectively. Therefore, only WPB (particularly for one row of tall perforations) and LPB may increase the buckling efficiency of a plate, where efficiency is the capacity-to-weight ratio. This is attributed to the redirection of stresses to the supported edges; similar behaviour may be seen for the perforated web of a steel section.

In the absence of a procedure to determine by which mode a perforated plate would buckle, several authors have proposed methods to find the elastic buckling load of such plates. In [4], an expression for the elastic buckling load of plates with multiple rows of perforations is developed. Despite this, it performs poorly for plates with $n_r > 1$ in the parametric domain investigated here. Overall, the prediction by [26] is most accurate for plates with $n_r > 1$, in particular for plates exhibiting WPB with $n_r > 1$ ($R^2 = 0.848$).

Equations to determine the local elastic buckling load for each buckling mode identified with the algorithm are then developed with the help of machine-learning-directed-regression-analysis. We establish first a new governing geometrical parameter τ for plates with $n_r > 1$ and a corresponding equation (Eq. (16)) valid for WPB, INT and ESB; and second, a new governing geometrical parameter ω for plates with $n_r = 1$ and a corresponding equation (Eq. (19)) valid for WPB, INT and USB. Overall, the ratio of the local elastic buckling load appropriately predicted with either Eq. (16) or Eq. (19) to the value computed with FE has a mean of 1.00 with a COV of 0.093, with an overall R^2 coefficient of 0.840 for all 775 models

We show that in addition to a high R^2 test result for the WPB mode, Eq. (16) outperforms the equation proposed by [26] for the INT and ESB modes. Of the three modes, the R^2accuracy of the latter is however somewhat poorer. Similarly, Eq. (19) surpasses the R^2 test performance of current predictions (although this is less than that for plates with $n_r > 1$). Yet, the R^2accuracy of plates with USB deformation is slightly worse than that found for the INT or WPB. Therefore, when the USB or ESB mode is identified with the algorithm, a greater model factor γ should be applied to the predicted elastic buckling load. A model factor $\gamma = 1.17$ is proposed for all buckling modes, with the exception of LPB. This was determined for $\alpha = 0.05$, i.e. 95 % of buckling load design predictions ($N_{cr,d}$) possess a buckling load less than the computed value ($N_{cr,FEM}$), and are thus conservative.

Furthermore, we conclude that the LPB buckling mode follows a distinct behaviour and Eq. (19) should not be used for this buckling mode; the elastic buckling load prediction for this mode should be a focus for future research. Lastly, both new geometrical parameters τ and ω are independent of the spacing between perforations. This suggests that they may be applicable to other arrangements such as staggered or irregular arrays, which will also be explored in future research.

CRediT authorship contribution statement

Elenor Naraidoo: Writing – review & editing, Writing – original draft, Resources, Investigation. **Barbara Rossi:** Writing – review & editing, Supervision.

Declaration of competing interest

The authors declare that they have no known competing financial interests or personal relationships that could have appeared to influence the work reported in this paper.

Data availability

Data will be made available on request.

References

[1] M.P. Kulatunga, M. Macdonald, Investigation of cold-formed steel structural members with perforations of different arrangements subjected to compression loading, Thin-Walled Struct. 67 (2013) (2013) 78–87.
[2] J. Ketsi, Local and distortional buckling of perforated steel wall studs. Dissertaion for the degree of Doctor of Science in Technology, Helsinki University of Technology, 2000.
[3] C.D. Moen, B.W. Schafer, Elastic buckling of thin plates with holes in compression or bending, Thin-Walled Struct. 47 (2009) 1597–1607.
[4] F. Smith, C.D. Moen, Finite strip elastic buckling solutions for thin-walled metal columns with perforation patterns, Thin-Walled Struct. 2014 (79) (2014) 187–201.
[5] Y. Guo, X. Yao, Experimental study and effective width method for cold-formed steel lipped channel stud columns with holes, Adv. Civ. Eng. 2021 (2021).
[6] AISI S100-16, North American Specification for the Design of Cold-Formed Steel Structural Members, American Iron and Steel Institute, Washington DC, USA, 2022.
[7] AS/NZS 4600, "Cold-formed steel structures," Standards Australia /Standards New Zealand, Sydney, 2018.
[8] SANS 10162-4:2011, The Design of Cold-Formed Stainless Steel Structural Members, South African Bureau of Standards, Pretoria, 2011.
[9] AISI, Design Strength Method (DSM) Design Guide, American Iron and Steel Institute, USA, 2006.
[10] G. 50017-2017, Technical Code for Cold-Formed Thin-walled Steel Structures, Chinese National Standard, Beijing, China, 2017.
[11] EN 1993-1-5, Eurocode 3: Design of steel structures - Part 1-5: Plated structural elements, European Committee for Standardisation (CEN), Brussels, 2006.
[12] K. Kathage, T. Misiek, H. Saal, Stiffness and critical buckling load of perforated sheeting, Thin-Walled Struct. 2006 (44) (2006) 1223–1230.
[13] A.M. Sweedan, K.M. El-Sawy, Elastic local buckling of perforated webs of steel cellular beam-column elements, J. Constr. Steel Res. 2011 (67) (2011) 1115–1127, 1 February.
[14] A. Matloub, S. Hassan, I. Hussein, A. Yousef, Flexural strength of steel girders with perforated web and tubular compression flange, Struct. Build. (ICE Publ.) (2023).
[15] B. Salhab, Y.C. Wang, Equivalent thickness of cold-formed thin-walled channel sections with perforated webs under compression, Thin-Walled Struct. (2008) 823–838.
[16] X. Yao, X. Li, Y. Guo, Elastic buckling behaviour of thin plate with circle holes under axial compression, in: IOP Conference Series: Earth and Environmental Science, Vol. 283, 5th International Conference on Environmental Science and Civil Engineering (ESCE2019), Nanchang, China, 2019.
[17] G. Brando, G. De Matteis, Buckling resistance of perforated steel angle members, J. Constr. Steel Res. (2013) 52–61.
[18] C. Bernuzzi, F. Maxenti, European alternatives to design perforated thin-walled cold-formed beam-columns for steel storage systems, J. Constr. Steel Res. (2015) 121–136.
[19] Z. Yao, K.J.R. Rasmussen, Perforated cold-formed steel members in compression. I: parametric studies, J. Struct. Eng. 143 (2016).
[20] C.D. Moen, B.W. Schafer, Direct strength method for design of cold-formed steel columns with holes, J. Struct. Eng. 137 (2011).
[21] S. Adany, Constrained shell finite element method for thin-walled members with holes, Thin-Walled Struct. (2017) 41–56.
[22] S. Minera, M. Patni, A. Pirrera, P.M. Weaver, Buckling-resistant topological design using sensitivities to variations in localised nominal stiffness, Thin-Walled Struct. 167 (2021) (2021).
[23] J.B. Gracia, F.G. Rammerstorfer, Increase in buckling loads of plates by introduction of cutouts, Acta Mech. 239 (2019) (2019) 2873–2889.
[24] C.D. Moen, B.W. Schafer, Elastic buckling of cold-formed steel columns and beams with holes, Eng. Struct. (2009) 2812–2824.
[25] E. Naraidoo, Z. You, B. Rossi, Elastic buckling of slender steel plates wtih perforations. Nordic Steel, Lulea, 2024.
[26] I.C. Scheperboer, E. Efthymiou, J. Maljaars, Local buckling of aluminium and steel plates with multiple holes, Thin-Walled Struct. 2016 (99) (2016) 132–141.
[27] J. Davies, P. Leach, A. Taylor, The design of perforated cold-formed steel sections subject to acial load and bending, Thin-Walled Struct. 1997 (29) (1997) 141–157.
[28] A.B. Sabir, F.Y. Chow, Elastic buckling of plates containing eccentrically located circular holes, Thin-Walled Struct. 4 (1986) (1986) 135–149.
[29] C.D. Moen, B.W. Schafer, Experiments on cold-formed steel columns with holes, Thin-Walled Struct. 2008 (46) (2008) 1164–1182.
[30] W.P. Vann, Compressive Buckling of Perforated Plate Elements, Missouri, 1971.
[31] T.M. Shakerley, C.J. Brown, Elastic buckling of plates with eccentrically positioned rectangular perforations, Int. J. Mech. Sci. 38 (1996) (1996) 825–838.

[32] K. El-Sawy, A.S. Nazmy, Effect of aspect ratio on the elastic buckling of uniaxially loaded plates with eccentric holes, Thin-Walled Struct. 2001 (39) (2001) 938–998.
[33] M.A. Komur, M. Sonmez, Elastic buckling of rectangular plates under linearly varying in-plane normal load with a circualr cutout, Mech. Res. Commun. 2008 (35) (2008) 361–371.
[34] W.-W. Yu, C.S. Davis, Buckling Behavior and Post-Buckling Strength of Perforated Stiffened Compression Elements, Missouri, 1971.
[35] R. Narayanan, F.Y. Chow, Ultimate capacity of uniaxially compressed perforated plates, Thin-Walled Struct. 1984 (2) (1984) 241–264.
[36] S.W.-K.S. Timoshenko, Theory of Plates and Shells, 2nd Edition ed., McGraw-Hill, New York, 1959.
[37] Z.P. Bazant, L. Cedolin, Stability of Structures, World Scientific Publishing Co., London, 2010.
[38] ABAQUS, 11.2 Linear Perturbation analysis, ABAQUS, 2009. January[Online]. Available: https://classes.engineering.wustl.edu/2009/spring/mase5513/abaqus/docs/v6.6/books/gsa/default.htm?startat=ch11s02.html [Accessed 15 December 2023].
[39] K.M. El-Sawy, A.S. Nazmy, M.I. Martini, Elasto-plastic buckling of perforated plates under uniaxial compression, Thin-Walled Struct. 2004 (42) (2004) 1083–1101.
[40] C. Moen, Direct Strength Design of Cold-Formed Steel Members with Perforations, Johns Hopkins University, Baltimore, Maryland, 2008. Dissertation (Ph.D), Vols.
[41] python, “random - generate pseudo-random numbers,” python, 27 December 2023, Online]. Available: https://docs.python.org/3/library/random.html, 2023 [Accessed 27 December].
[42] scikit, “scikit-learn Machine Learning in Python,” scikit-learn, 2025 [Online]. Available, https://scikit-learn.org/stable/, 2025 [Accessed 20 03].
[43] SciPy, SciPy API >optimisation and root finding (scipy.optimiz) >minimize, SciPy (2025) [Online]. Available, https://docs.scipy.org/doc/scipy/reference/generated/scipy.optimize.minimize.html [Accessed 20 03 2025].